Splinter Session on Cool Cloudy Atmospheres: Theory and Observations

Adam J. Burgasser[1], Jacqueline Radigan[2], Abhijith Rajan[3], Stan Metchev[4], Adam Showman[5], Xi Zhang[5], Beth Biller[6], Esther Buenzli[7], Mark Marley, Kay Hiranaka[9], William M. J. Best[10], Caroline Morley[11], David Sing[12], Daniel Apai[13], & Michael Gillon[14]

[1] *UC San Diego, Center for Astrophysics and Space Sciences, Mail Code 0424, 9500 Gilman Drive, La Jolla, CA 92093-0424, USA*

[2] *Space Telescope Science Institute, 3700 San Martin Drive, Baltimore MD 21218, USA*

[3] *Arizona State University, School of Earth & Space Exploration, Interdisciplinary Science & Technology Building 4 Rm 542, Tempe, AZ 85287, USA*

[4] *The University of Western Ontario, Department of Physics and Astronomy, 1151 Richmond Avenue, London, ON N6A 3K7, Canada*

[5] *Lunar and Planetary Lab, University of Arizona, Tucson, AZ 85721-0092 USA*

[6] *Institute for Astronomy, The University of Edinburgh Royal Observatory, Blackford Hill, Edinburgh EH9 3HJ, UK*

[7] *Max-Planck Institute for Astronomy, Koenigstuhl 17, D-69117 Heidelberg, Germany*

[8] *NASA Ames Research Center, MS-245-3, Moffett Field, CA 94035, USA*

[9] *Hunter College, Department of Physics and Astronomy, 695 Park Ave, New York, NY 10065 USA*

[10] *University of Hawaii, Institute for Astronomy, 2680 Woodlawn Drive, Honolulu, HI 96822 USA*

[11] *UC Santa Cruz, Astronomy & Astrophysics Department, 1156 High Streat, Santa Cruz, CA 95064 USA*

[12] *Astrophysics Group, School of Physics, University of Exeter, Stocker Road, Exeter EX4 4QL, UK*

[13] *The University of Arizona, Department of Astronomy, 933 N. Cherry Avenue, Tucson, AZ 85721, USA*

[14] *Institute of Astrophysics and Géophysique, Université of Liège, allée du 6 Août, 17, B-4000 Liège, Belgium*

1. Splinter Motivation

Condensate formation is a key process in planetary and brown dwarf atmospheres, influencing photospheric gas chemistry and composition, modulating long-term thermal evolution, and driving short-term variability. Condensate grain opacity strongly influences the near-infrared spectral energy distributions of ultracool (UCD) M, L, T, and (possibly) Y dwarfs; and cloud evolution plays a major role in triggering (and possibly delaying) the L dwarf/T dwarf transition. As a tracer of atmospheric dynamics, condensate clouds allow us to measure the rotation and orientation of a cool dwarf, while long-term variations may reflecting circulation and atmospheric structure changes.

In the short time since the Clouds in Brown Dwarfs and Giant Planets Splinter Session in Cool Stars 17 (Metchev et al. 2013), major observational results have emerged in the characterization of exoplanet and brown dwarf clouds, including the completion of large-scale, high-precision near- and mid-infrared variability surveys; detection of new "large-amplitude" variables; detection of phase variation in multi-wavelength and spectroscopic variability; evidence of clouds in exoplanet atmospheres; identification of exoplanets spanning the L/T (cloud) transition; and study of cloud differences between exoplanets and brown dwarfs. These results have been coupled with theoretical advancements in 3D atmospheric dynamics (e.g., global circulation models applied to brown dwarf atmospheres), the identification of new cloud species, and improved modeling of cloudy atmospheres.

The goal of this splinter session was to disseminate and discuss these advancements through a series of short talks highlighting recent observational and theoretical work. The talks were chosen to focus on four primary questions:

1. What is the nature of cloud-induced variability, and how does atmospheric dynamics drive these variations?

2. How does cloud structure vary among nearby cool dwarfs, and what determines these variations?

3. How do clouds influence the thermal and atmospheric evolution of brown dwarfs, particularly at the L/T transition?

4. How do clouds differ in exoplanet and brown dwarf atmospheres, and why?

The following sections summarize the contributions from our speakers. The presentations themselves can be accessed at the splinter website[1] and viewed in their entirety on YouTube.[2]

---

[1] http://www.browndwarfs.org/cs18/

[2] Part 1 can be viewed at https://www.youtube.com/watch?v=Bd7vdawpobs; part 2 can be viewed at https://www.youtube.com/watch?v=HtWoexgYRsA.

2. As the Dust Settles: Using Time-domain Observations to Reveal Cloud Structure at the L/T Transition (Jacqueline Radigan)

The combination of condensate clouds and rapid rotation has long motivated searches for weather phenomena in UCD atmospheres. Pioneering work dating back to 1999 suggested that variability is quite common for UCDs (e.g. Tinney & Tolley 1999; Bailer-Jones & Mundt 1999; Gelino et al. 2002; Koen 2003; Koen et al. 2004; Enoch et al. 2003; Goldman et al. 2008; Clarke et al. 2008). Yet early studies were ambiguous: detections were often low-amplitude and/or lacking periodicity, and the mechanisms responsible remained unclear. Variability was often described as being marginal or intermittent, and no population of reliable variables, suitable for detailed follow-up, were identified. Observations made in the past 5 years, utilizing continuous monitoring strategies, better instruments, and larger telescopes have demonstrated conclusive, and repeatable variability for UCDs across the entire M-L-T sequence.

The first compelling, multi-epoch detection came from Artigau et al. (2009) who found the T2.5 dwarf SIMP 0136 to vary with an amplitude of up to 8% in the J band, with a $\sim$2.5 hr period. Reports of large-amplitude variability in several other early T-dwarfs followed: 26% variability of the T1.5 dwarf 2M2139+02 (Radigan et al. 2012), 3% variability of the T1/T1 binary SDSS1052+44 (Girardin et al. 2013), $\sim$10% variability of the T0.5 component of the Luhman 16 binary (Gillon et al. 2013; Biller et al. 2013; Burgasser et al. 2014, see also contribution of B. Biller herein), and several percent variability of two additional T2 dwarfs (2M0758+32 and SIMP1629+03; Radigan et al. 2014). At the same time, sensitive ground- and space-based surveys have found convincing low-level variability for brown dwarfs at all spectral types. Extrapolations from space based surveys suggest that every brown dwarf has a patchy photosphere to some degree (Buenzli et al. 2014, Metchev et al., submitted).

2.1 Population Statistics and the L/T Transition

The early T-dwarf variables, which occupy the milieu of the L/T transition color reversal, are distinguished by the large amplitudes of their variations at near-infared (NIR) wavelengths—particularly at J-band—presumably caused by larger and/or higher contrast cloud features at these spectral types. A survey of 57 L and T dwarfs by Radigan et al. (2014) found the increase in large-amplitude variability (peak-to-trough amplitudes >2%) to be highly significant (Figure .1). A dynamic disruption of the cloud layer, leading to localized regions of low condensate opacity (allowing photons to emerge from deeper in the photosphere), may explain or contribute to observed features of the L/T transition including the abrupt NIR color reversal and J-band brightening from late-L to mid-T spectral types (Ackerman & Marley 2001; Burgasser et al. 2002b; Marley et al. 2010; Dupuy & Liu 2012; Faherty et al. 2012).

2.2 Characteristics of L/T Transition Variables

The large-amplitude early-T variables lend themselves to detailed multi-wavelength follow-up (e.g. Artigau et al. 2009; Radigan et al. 2012; Apai et al. 2013; Biller et al. 2013; Metchev et al. 2013; Burgasser et al. 2014). Variability as a function of wavelength is remarkably similar for the L/T transition dwarfs monitored to date. Artigau et al. (2009); Radigan et al. (2012); Burgasser et al. (2014) all find flux ratios of $\Delta K/\Delta J \sim 0.5$. Spectroscopic

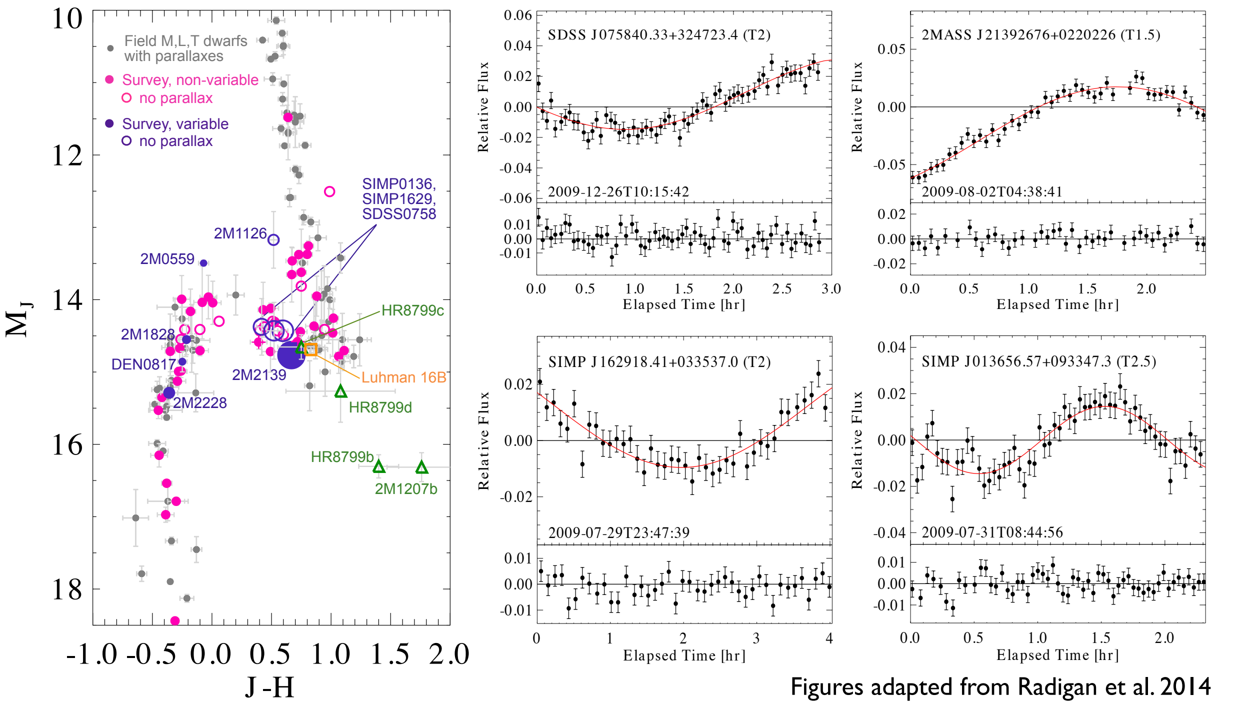

Figure .1: *Left:* Color magnitude diagram for variable and non-variable survey targets (pink and purple points respectively) from Radigan et al. (2014). Symbol size scales with observed peak-to-trough amplitude (range is 0.6%-9%). Open circles mark targets without parallax data, for which spectroscopic parallaxes were found using the spectral type-absolute magnitude relationship defined by Dupuy & Liu (2012). Field ultra cool dwarfs with parallaxes from the database of Trent J. Dupuy are shown as grey circles. *Right:* Light curves for 4 large-amplitude variables at the L/T transition, with light curves of similar-brightness reference stars shown below for comparison.

monitoring with WFC3 of SIMP 0136 and 2M2139 (Apai et al. 2013) reveals variability that very weakly decreases as a function of wavelength across the $1.1-1.7\mu$m continuum, with the exception of the water band which varies (in the relative sense) at a level of $\sim$50% that of the continuum. The observed wavelength dependence of the variability is shallower than predicted by a model consisting of clouds and clearings; the most likely explanation is that we do not ever peer into 100% cloud-free regions, but rather observe the contrast between regions of thick and thin clouds.

In contrast to the T6.5 dwarf 2M2228-43 which shows evidence for wavelength-dependent phase-shifts (Buenzli et al. 2012), WFC3 variability for L/T transition dwarfs is correlated across the entire wavelength rage observed (however, see the contribution of B. Biller herein). A factorization of the time series into principle components (or alternatively non-negative components, as shown in Figure .2) reveals that the variability (within uncertainties) is entirely described by linear combinations of only two surface types.

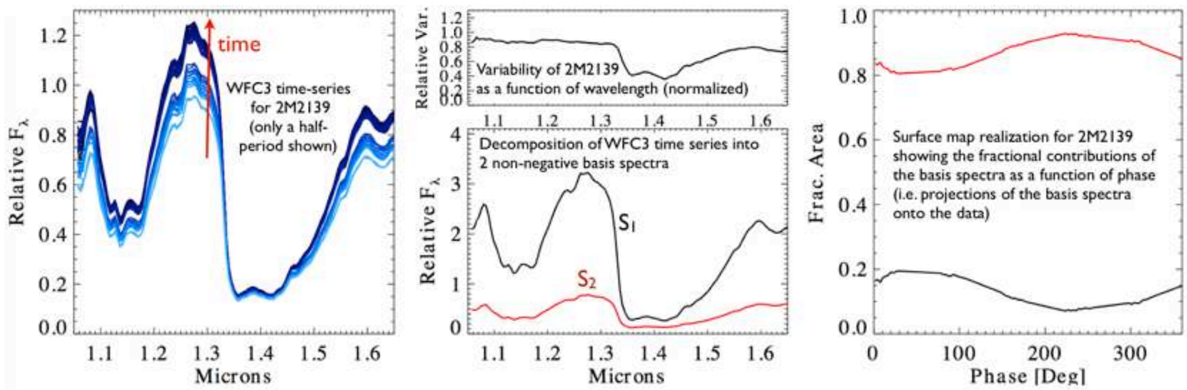

Figure .2: An example of WFC3 data taken for the highly variable T1.5 dwarf 2M2139 (Apai et al. 2013). *Left*: a time series of spectra showing brightness changes over a half rotation period. *Middle:* the top panel shows the level of variability as a function of wavelength (normalized at 1.1 micron). The bottom panel shows a non-negative matrix factorization of the time series into two non-negative basis spectra, S_1 and S_2 such that a spectrum at any time is given by $S(t) = c_1(t)S_1 + c_2(t)S_2$. *Right:* A surface map realization for 2M2139 showing the fractional contributions of each surface component c_1 and c_2 as a function of phase.

Dynamically, the L/T transition objects exhibit complex behaviors with amplitudes and light curve morphologies that evolve on timescales of hours to years (Artigau et al. 2009; Radigan et al. 2012; Metchev et al. 2013; Gillon et al. 2013). A possible correlation between variability amplitude and rotation period, consistent with feature sizes that scale with the Rhines length, has been proposed by Apai et al. (2013) and Burgasser et al. (2014), but requires observations of additional targets (preferably at multiple epochs) to test whether this pattern holds for a larger population.

3. The Brown Dwarf Atmosphere Monitoring (BAM) Project: Studying the Coolest Atmospheres (Abhijith Rajan)

We present the results of two complementary Brown dwarf Atmosphere Monitoring programs (BAM-I & II) characterizing sub-stellar L, T, and Y-dwarfs. The study (BAM-I) monitored 69 L0-T8 brown dwarfs with the sample equally split across the early-L, L/T transition, and late-T dwarfs (Wilson et al. 2014). All the targets were monitored at the New Technology Telescope at La Silla, with the targets being observed in pairs, over 14 nights. The observing strategy resulted in each target being monitored for ∼2-4 hrs. The survey detected 14 variables, including nine new targets while confirming five literature variables. The survey data does not show any trend in the frequency of variability with spectral type, with variables detected across the full sample spectral range. Adjusting the boundaries of the transition did not change this conclusion.

The variables identified as part of the BAM-I survey are currently being followed-up with the NTT via an ESO large program. The BAM-III follow-up observations are multi-

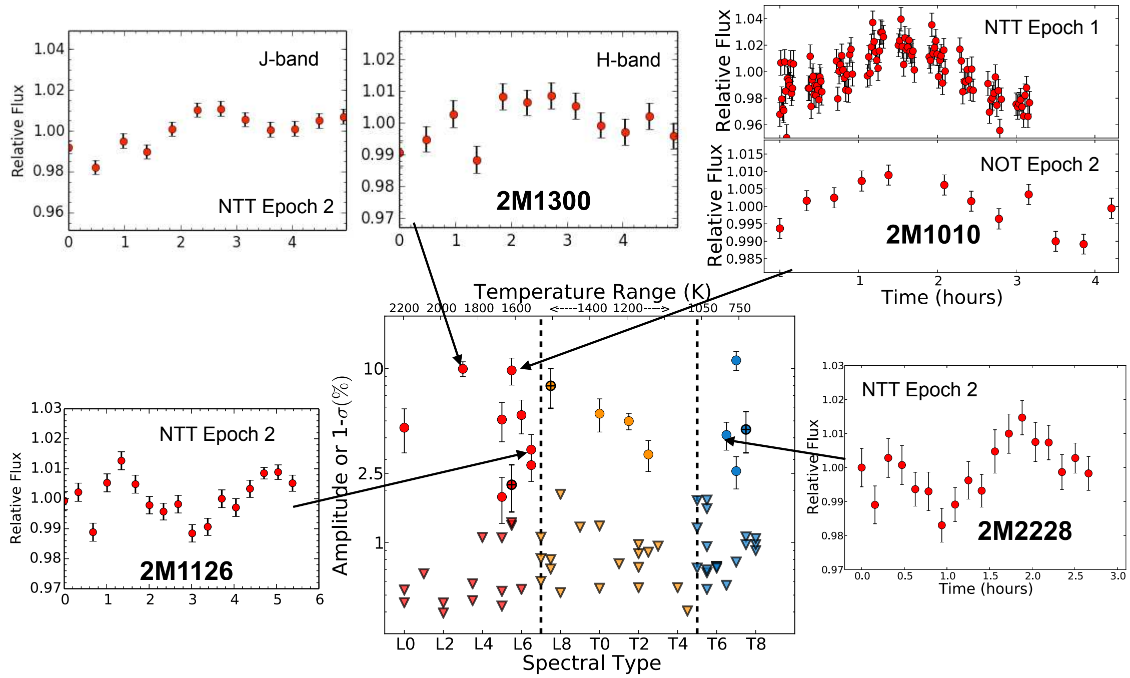

Figure .3: Presenting preliminary BAM-III follow-up variability light curves. The data is being collected over multiple wavelengths spanning the near-IR intended to characterize the BAM-I variable brown dwarfs using broadband photometry over multiple epochs.

wavelength with concurrent J & H-band data being taken typically and where possible J, H, and K. Additionally, each variable is being monitored at least two to three times over the duration of the program. Preliminary light curves from the BAM-III program are presented in Figure .3. By comparing the BAM-I results for targets that have been previously monitored we find that approximately 40% of these targets switched states between constant and variable. This suggests that multi-epoch observations are invaluable in properly characterizing brown dwarf atmospheres.

The BAM-II pilot study monitored 4 late-T/Y dwarfs, including the planetary mass object Ross 458C (Rajan et al. 2014). The three brightest targets had multi-epoch monitoring. Two of the targets appeared to remain constant within the limits of the data in all the epochs. One target, WISE0458, showed remarkably high amplitude variations in the first epoch (∼16%) and two years later appears constant. We are continuing to monitor this source with both ground- and space-based instrumentation to see if the target continues to show long-term variability.

Combining the BAM-I and BAM-II results, we see that 13 objects switch between having variable and constant lightcurves (including WISE0458). Additionally, there appears to be a preliminary trend in the data, where the constant targets might be concentrated near the clear atmosphere tracks and the variables appear to have cloudier atmospheres based on model atmospheres of cool brown dwarfs (Saumon et al. 2012; Morley et al. 2012). We are currently undertaking a larger and more complete survey of cool mid- to late-T dwarfs to investigate this potential correlation.

4. Space-based Variability Studies Indicate that Spots are Ubiquitous on Brown Dwarfs (Stan Metchev)

I present results from the *Weather on Other Worlds Spitzer* Exploration Science program to investigate cloud-induced photometric variability in L and T dwarfs. We surveyed 45 objects with spectral types approximately uniformly distributed between L3 and T8, covering a broad range of $J-K_s$ colors and surface gravities. We find that 14/25 ($56\% \pm 10\%$, 1-σ confidence interval) of our L3–L9.5 dwarfs are variable, with peak-to-peak amplitudes between 0.2% and 1.5%, and 6/20 ($30\%^{+11\%}_{-9\%}$) of our T0–T8 dwarfs are variable with amplitudes between 0.7% and 4.6%. After correcting for sensitivity, we find that $85\%^{+10\%}_{-15\%}$ of L dwarfs vary with $\geq$0.2% peak-to-peak amplitudes, and $40\%^{+20\%}_{-19\%}$ of T dwarfs vary by $\geq$0.4%. Given viewing geometry considerations, we conclude that photospheric heterogeneities causing >0.2% 3–5μm flux variations are present on virtually all L dwarfs, and probably on most T dwarfs. A third of L dwarf variables show irregular light curves, which indicates that L dwarfs are more likely to have multiple spots that evolve on time scales of a single rotation period. We detect an increasing trend in the maximum amplitude over the entire range of spectral types, revealing a potential for greater temperature contrasts in the T dwarfs than in the L dwarfs. The objects' rotation periods, assumed to be the dominant temporal component of the observed variability for most targets, range between 1.4 h and >20 h, where the upper end of the range is limited by the 21 h duration of our uninterrupted monitoring of each target. A third of the periodicities are on scales >10 h, indicating that slowly-rotating brown dwarfs are not unusual. We find a significant correlation between low-gravity and/or dusty atmospheres and high amplitude of variations in L3–L5.5 dwarfs. Although we can not confirm whether low surface gravity also leads to a higher incidence of variables, the evidence for higher amplitudes at low gravities is very promising for the characterization of young directly imaged extrasolar planets through variability monitoring.

5. Atmospheric Dynamics of Brown Dwarfs (Adam Showman)

A variety of evidence now points to vigorous atmospheric circulations on brown dwarfs. First, clouds, long inferred from infrared spectra, imply the existence of atmospheric mixing, since in the absence of mixing such cloud particles would settle out of the observable atmosphere. Second, disequilibrium chemistry likewise provides evidence for vertical mixing. In particular, the CO abundance on many brown dwarfs inferred from IR spectra exceeds the chemical equilibrium abundance, implying that CO is transported from deep levels (where it is chemically stable) to the atmosphere on timescales sufficiently fast to prevent it from relaxing back into equilibrium. On cooler brown dwarfs, NH_3-poor air from depth likewise mixes into the upper troposphere, causing a deficit of NH_3 relative to chemical equilibrium. From the chemical kinetics, estimates of the vertical mixing rates can be made. Third, as emphasized in other parts of this article, many brown dwarfs are highly variable in the near-IR, suggesting the existence of cloudy and less-cloudy patches that come into and out of view as the brown dwarf rotates. Light curves typically change shape over days, implying that the pattern of cloud patchiness evolves over time. Fourth, maps of the nearby brown dwarf Luhman 16B, constructed from Doppler imaging, indicate a patchy surface, probably

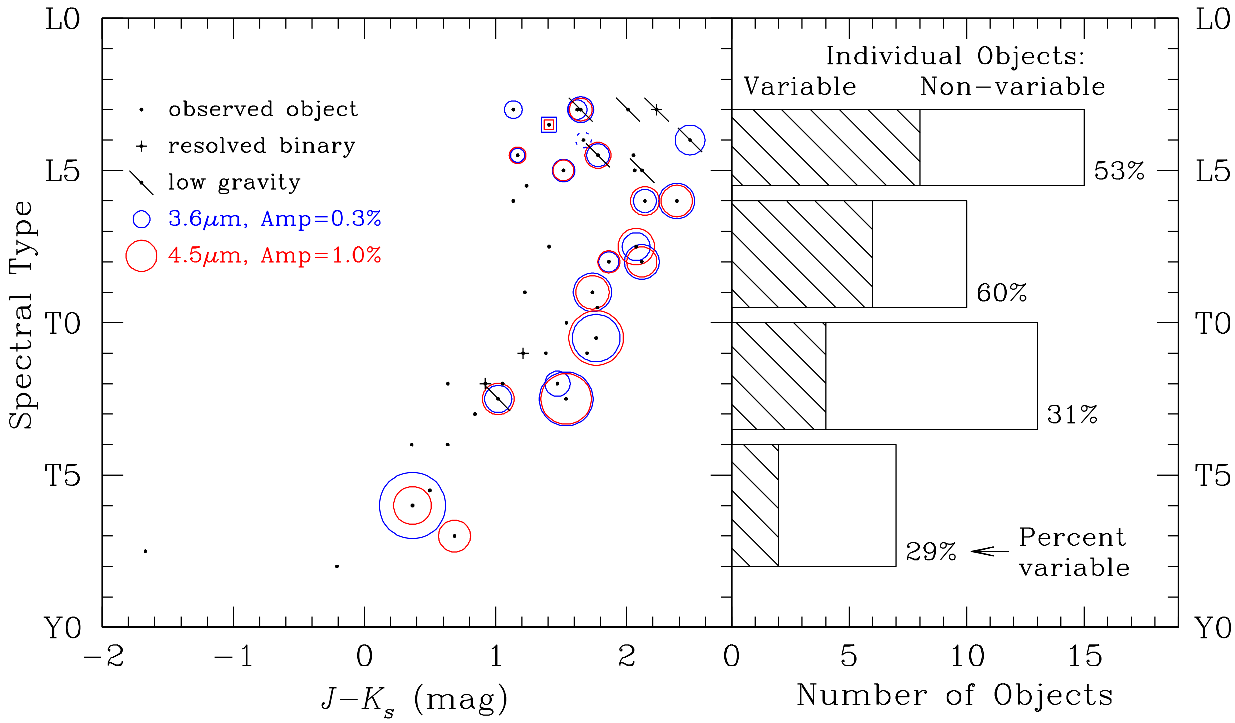

Figure .4: **Left:** Color, spectral type, and variability distribution of our 44 L3–T8 targets. Circles enclose the variable targets, with the area of the circle proportional to the variability amplitude in the IRAC [3.6] band (blue) or [4.5] band (red). The dashed blue circle encloses object 2MASS J175334518–6559559 (L4), which displays only a linear trend at [3.6], and does not have a well defined amplitude. The previously known magnetically active L3.5 dwarf 2MASSW J0036159+182110, not part of the unbiased sample, is variable and shown with concentric squares. Known close binaries are marked with +. Inclined bars denote low-gravity objects, including six L3–L5 dwarfs (one a close binary) and the T2.5 dwarf HN Peg B. **Right:** Distribution and frequency of [3.6] or [4.5] variability of individual objects in our unbiased sample as a function of spectral type. The previously known magnetically active L3.5 variable 2MASSW J0036159+182110 is not included in the statistics.

caused by patchy clouds and an associated large-scale atmospheric circulation (Crossfield et al. 2014). See Showman & Kaspi (2013) for a more detailed survey and references.

What is the dynamical regime of such an atmospheric circulation? Brown dwarfs rotate rapidly; for typical rotation periods of ∼2–12 hours, the atmospheric dynamics is rotationally dominated, with Rossby numbers that are much less than one (Showman & Kaspi 2013). The absence of external irradiation on most brown dwarfs implies that the there are no (strong) externally imposed gradients of temperature, which implies that the main mechanism for the atmospheric circulation on solar-system planets and close-in exoplanets—namely, transport of heat from equator to poles or day to night—is ruled out for brown dwarfs. But brown dwarfs lose prodigious heat and their interiors vigorously convect. Freytag et al. (2010) showed that this convection will drive a wide spectrum of gravity waves in the stably stratified atmosphere that overlies the convection region. While not modeled by Freytag et al., solar-system experience shows that Rossby waves are also likely. Showman & Kaspi (2013) proposed that the breaking, absorption, and dissipation of these waves in the overlying stratified atmosphere will drive a vigorous, large-scale atmospheric circulation, which may bear some resemblance to the circulation in the stratospheres of solar-system planets.

Zhang & Showman (2014) presented one-layer shallow-water models of the atmospheric circulation on brown dwarfs to investigate the extent to which the circulation modulates into band and zonal jets, like Jupiter and Saturn, or whether the circulation instead consists primarily of isotropic turbulence and vortices. They found that, under conditions of strong rotation and weak radiative damping, the circulation exhibits a banded pattern, like Jupiter. But when the radiative damping is strong, the damping can remove turbulent energy before it has time to reorganize into zonal jets. Since many brown dwarfs will have short radiative time constants, this suggests that at least some brown dwarfs may not be banded.

I have presented preliminary models to extend this analysis to three dimensions. I performed global, 3D numerical simulations of the atmospheric flow using the MITgcm, which is a state-of-the-art general circulation model (GCM) that has been used to investigate the atmospheres of solar-system planets and hot Jupiters, Neptunes, and super Earths. The model represents a rapidly rotating (5-hour period) brown dwarf with a radius equal to Jupiter's radius. The domain represents the stratified atmosphere and extends from 0.01 bars at the top to 10 bars at the bottom. We parameterized convection by adding isotropic thermal perturbations, varying randomly in time over some specified correlation timescale, at the bottom of the domain (pressures exceeding 5 bars). In the simulations described, these perturbations exhibit a total horizontal wavenumber of 20. Radiative transfer is parameterized with Newtonian cooling, which relaxes the local temperature toward a specified radiative-equilibrium temperature (which varies with height but not latitude or longitude) over a specified radiative time constant. We systematically varied the radiative time constant in a series of simulations to determine its influence on the circulation.

In these models, the convective perturbations at the bottom of the domain trigger large-scale waves, which propagate upward into the stratified atmosphere. Interaction of these waves with the mean flow drives turbulence, zonal jets, and in some cases stable, long-lived vortices. When the radiative time constant is long (10^6 or 10^7 sec), the main feature is a sequence of alternating zonal jets that extend over most latitudes. At intermediate radiative time constants (10^5 sec), jets still exist, but only equatorward of $\sim 45°$ latitude. At short radiative time constants (10^4 sec), a banded flow pattern exists only close to the equator (latitude $< 15°$), with weak, quasi-isotropic turbulence covering the higher latitudes. This transition from jets to turbulence is analogous to that shown in Zhang & Showman (2014). Interestingly, in the 3D simulations, the transition occurs at different radiative time constants at different latitudes; it is easier to suppress jets at high latitudes than at the equator. This tendency can be understood with simple scaling arguments. In a geostrophic, low-Rossby-number flow, the horizontal divergence is significant at the equator but nearly zero at the poles. The greater horizontal divergence at low latitudes permits greater vertical motion there, allowing greater vertical entropy advection, greater temperature fluctuations, and greater Rossby wave generation. The result is zonal jets that are harder to suppress at low latitudes than high latitudes.

We are continuing to explore the parameter space and will present detailed results in a forthcoming paper.

6. Atmospheric Circulation of Brown Dwarfs: Jets, Vortices, and Time Variability (Xi Zhang)

Under the conditions of fast rotation, strong radiative dissipation and no external stellar flux, brown dwarfs occupy a unique corner of the parameter space of atmospheric dynamics theories. Here we ask: do the atmospheres of the brown dwarfs exhibit east-west jet patterns similar to those that exist on both the gas giants in our solar system and the close-in extra-solar giant planets? Or are brown dwarf atmosphere dynamics dominated by isotropic turbulence and vortices instead? The answer is crucial for the interpretation of observed time variability of L/T dwarfs, as well as being of fundamental theoretical interest. We introduce an idealized global two-dimensional (2D) shallow-water model to study the atmospheric circulation on brown dwarfs. These are the first global numerical simulations of the dynamics in the stratified atmospheres of brown dwarfs. We explore two schemes for the spatial and temporal structure of the convective forcing. Atmospheres are randomly forced by either local perturbations ("thunderstorms") with different size, strength, and lifetime (local pulse forcing), or spherical harmonics with random forcing amplitude (global spectral forcing).

6.1 Jets Versus Vortices

In Figure .5 we show two idealized simulations, with a rotation period of 1.6 hours ($\Omega = 1.1 \times 10^{-3}$ s) and an equilibrium geopotential of 5×10^5 m^2 s^{-2}. Under conditions of strong internal heat flux and weak radiative dissipation, east-west jets spontaneously emerge from the interaction of atmospheric turbulence with the planetary rotation (upper panel). When the internal heat flux is weak and/or radiative dissipation is strong, turbulence injected into the atmosphere damps before it can self-organize into jets, leading to a flow dominated by isotropic turbulence and vortices instead (lower panel). In order to systematically investigate the jet-vortex dichotomy, we performed several hundred simulations over a wide range of forcing and dissipation parameters. We present a scaling law as a quantitative criterion for the emergence of jets versus vortices on gas giants and brown dwarfs (Fig. 2 in Zhang and Showman 2014). We conclude that the emergence of jet structure in a shallow water system is largely controlled by the energy injection rate and dissipation timescale.

6.2 Light Curve Evolution

We use the global shallow-water model to diagnose the long-term system behavior of brown dwarf atmospheres. Both the short-term and long-term behavior of our simulations, from hours to years, can help illuminate current and upcoming infrared light curve observations over various timescales (e.g., Artigau et al. 2009; Apai et al. 2013). We found that the brown dwarf atmosphere is dominated by the rotational modulation in short-term light curves, with lightcurve shapes that vary from single to multi-peaked periodic structures and amplitudes of a few percent, qualitatively consistent with recent observed infrared flux variations of brown dwarfs (see Fig. 4 in Zhang and Showman 2014).

7. Weather on the Nearest Brown Dwarfs: Resolved Simultaneous Multiwavelength Variability Monitoring of Luhman 16AB (Beth Biller)

We have measured multiple epochs of MPG/ESO 2.2 m GROND simultaneous six-band ($r'i'z'JHK$) photometric monitoring of the closest known L/T transition brown dwarf binary

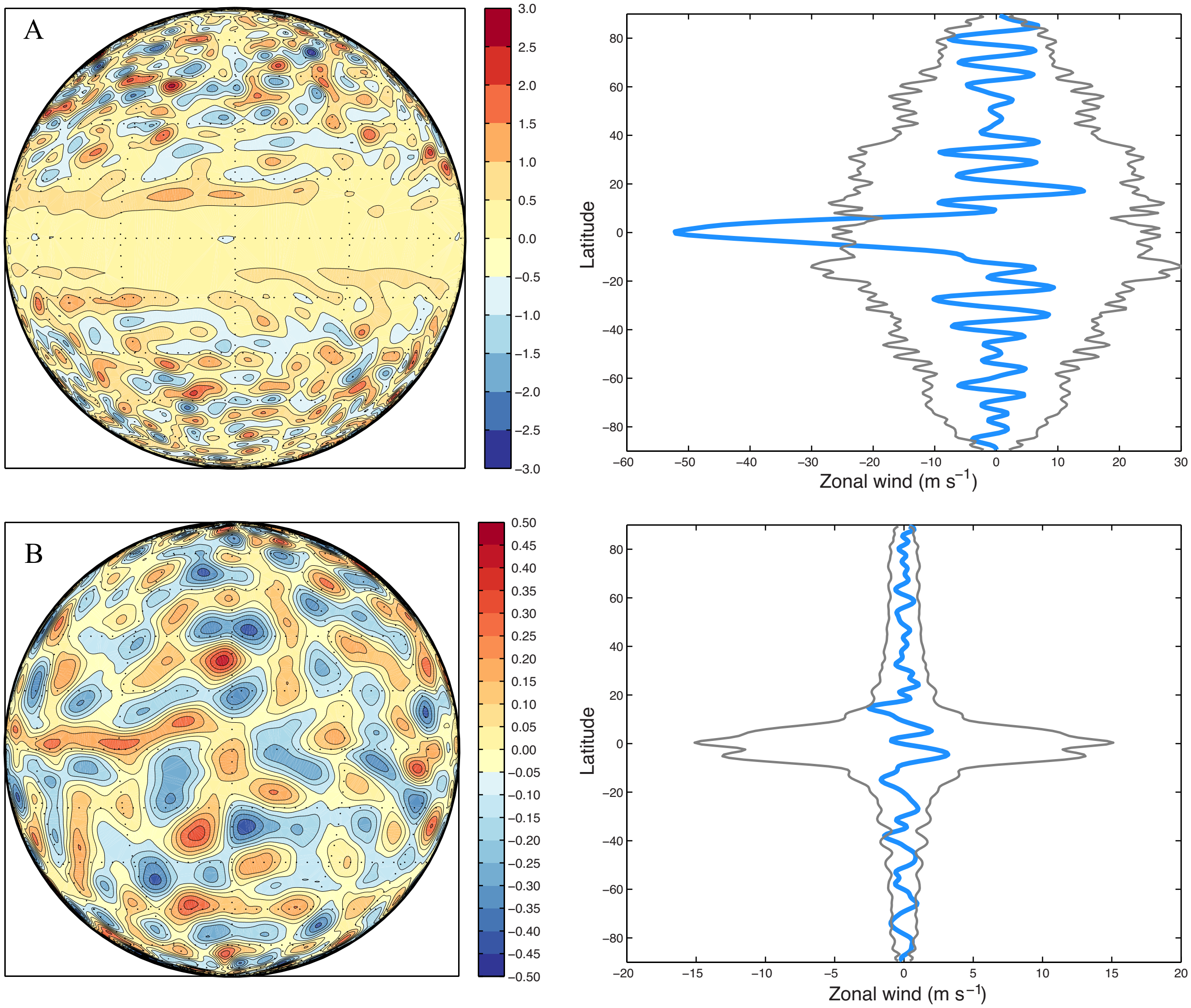

Figure .5: Two atmospheric regimes of brown dwarfs ($\Omega \sim 10^{-3}$ s) under forcing wavenumber 40. Figure is taken from Zhang & Showman (2014). Upper: jet case (case A) with longer radiative timescale (10^7 s) and forcing timescale (10^5 s), and with $s_m = 0.1\,\mathrm{m}^2\,\mathrm{s}^{-3}$; lower: vortex case (case B) with shorter radiative timescale (10^5 s) and forcing timescale (10^3 s), and $s_m = 0.5\,\mathrm{m}^2\,\mathrm{s}^{-3}$. Left: geopotential anomaly map (in units of 10^5 m^2 s^{-2}); right: zonal-mean zonal wind (blue) and standard deviation in longitude of the zonal wind at each latitude (gray). Both models have a small deformation radius of $\sim 10^3$ km.

Luhman 16AB. These include new epochs taken in February 2014. We report here the first resolved variability monitoring of both the T0.5 and L7.5 components. We note a number of robust trends in our light curves from April 2013. The r' and i' light curves appear to be anti-correlated with z' and H for the T0.5 component and in the unresolved light curve. In the defocussed dataset, J appears correlated with z' and H and anti-correlated with r' and i'; in the focused dataset, we measure no variability for J at the level of our photometric precision, likely due to evolving weather phenomena. In our focused T0.5 component light curve, the K band light curve displays a significant phase offset relative to both H and z'. We argue that the measured phase offsets are correlated with atmospheric pressure probed at each band, as estimated from one-dimensional atmospheric models. We also report low-amplitude variability in i' and z' intrinsic to the L7.5 component.

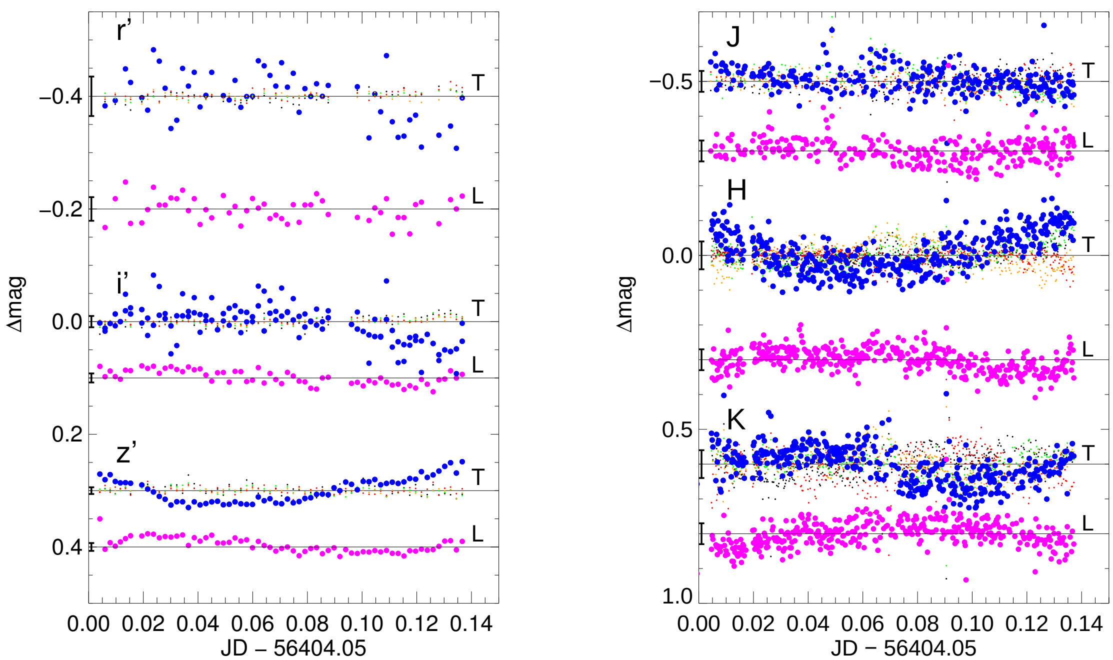

Figure .6: Single component light curves for Luhman 16 A and B from PSF-fitting photometry on UT 2013 April 22. Estimated error bars are plotted at the beginning of each light curve and example residual reference lightcurves (reference star - high S/N reference lightcurve) are plotted as small dots. Reprinted from Biller et al. (2013).

8. Patchy atmospheres beyond the L/T transition: Spectral variability of mid-T dwarfs (Esther Buenzli)

The sometimes patchy silicate clouds that dominate the photospheres of brown dwarfs at the L/T transition and can be responsible for significant near-infrared variability (e.g.,Artigau et al. 2009; Radigan et al. 2012) are thought to have disappeared from the visible photosphere for mid-T spectral types. Nevertheless, several variable mid-T dwarfs are currently known (Clarke et al. 2008; Radigan et al. 2014; Buenzli et al. 2014), although their J band variability amplitude is typically below 2%. It is possible that patchy sulfide clouds that may condense in these photospheres (Morley et al. 2012) could be responsible for some of that variability; another alternative are temperature fluctuations due to atmospheric circulation (Showman & Kaspi 2013; Zhang & Showman 2014; Robinson & Marley 2014).

The T6.5 dwarf 2MASS J22282889-431026 (hereafter 2M2228-43) shows complex wavelength dependent near-infrared variability (Buenzli et al. 2012) that is significantly different than the spectral variability of early T dwarfs (Apai et al. 2013). Simultaneous HST/WFC3 spectroscopic time-series from 1.1-1.68 μm and Spitzer IRAC 4.5 μm photometric time-series have revealed that light curves at different wavelengths not only have different amplitudes but also different phases, indicating complex three-dimensional atmospheric heterogeneities. The flux changes in the water band at 1.4 μm are approximately anti-correlated to those in the J and H band peak, while the light curves in the IRAC 4.5 μm channel and the 1.65 μm methane absorption band have intermediate phases. It appears that the phase shifts correlate with the pressure that is probed by a certain wavelength: light curves at wavelengths that predominantly probe higher altitudes (absorption bands) lag behind those that probe deeper (J and H band).

Not only are the phase shifts for 2M2228-43 unusual and different than those for the L/T transition dwarfs; the variability amplitude as a function of wavelength also behaves differently. For L/T transition dwarfs, the largest amplitudes are typically found in the J band or at shorter wavelengths, while the H band amplitude is of similar strength or only slightly lower (Radigan et al. 2012; Apai et al. 2013; Burgasser et al. 2014). The amplitude in the 1.4 μm water band is typically only about half of the J band amplitude. For 2M2228-43 however, we find the largest amplitude ($\approx$ 5% peak-to-valley) in the 1.4 μm absorption band, followed by the H band peak ($\approx$ 2.7%) and the J band peak and 1.65 μm methane band (both $\approx$1.9 %). The lowest amplitude is found in the IRAC band at 4.5 μm (1.5%).

Morley et al. (2014b) calculate the influence of patchy sulfide clouds and temperature hot spots on the emerging spectra of mid-T to Y dwarfs. For mid-T dwarfs ($T_{\rm eff} = 700 - 1000$ K) patchy sulfide clouds predict the highest variability amplitude in the Y and J bands, an intermediate amplitude in the H band, low amplitudes in the K and IRAC 4.5 μm band and almost no variations in the H_2O absorption band at 1.4 μm. Perturbations in the temperature-pressure profile on the other hand would predominantly introduce variability in the IRAC 3.6 μm band but practically none at all at 4.5 μm and in the J and H band peaks. Some variability is also predicted for the 1.4 μm water band.

Clearly, neither of these two options alone can explain the observed variability amplitudes for 2M2228-43. It is possible that patchy sulfide clouds deeper in the atmosphere are responsible for the J and H variability, while hot spots at lower pressure produce the larger 1.4 μm variability. This would imply large variability in the 3.6 μm IRAC channel, which preliminary results appear to support (Apai et al. in prep). Nonetheless, the fact that the H band peak amplitude is significantly higher than the J band peak amplitude cannot be explained by either of the two models. Nor do they explain why the 4.5 μm amplitude is not much lower than the J band amplitude but the phase is strongly shifted. Although the simultaneous presence of patchy clouds and hotspots may produce some out-of-phase variability, the phase-pressure correlation remains puzzling.

Robinson & Marley (2014) investigate whether phase shifts can occur when deep periodic temperature perturbations propagate upwards. Indeed this mechanism introduces a phase shift between the J, water and 4.5 μm bands. However, these phase shifts are on time-scales of the perturbation, which is typically longer than one rotation period (1.4 h for 2M2228-43). Rotational modulation would therefore still provide in-phase light curves that then slowly evolve. These models also do not yet incorporate the presence of clouds. 3D models that include patchy clouds and circulation may be required to understand the complex variability behavior of this brown dwarf.

2M2228-43 is being further monitored with Spitzer and HST within the STORMS exploration science program. Other variable mid-T dwarfs are now known that could provide a better idea on whether the complex spectral variability signatures of 2M2228-43 are unusual for mid-T dwarfs.

9. Cloud Models: Where do we go from Here? (Mark Marley)

The first wave of brown dwarf cloud models that arrived in the early 2000s attempted to account for the colors and spectral shape of the L dwarfs and the transition from L to T type dwarfs. These early models either parameterized the cloud or attempted to calculate cloud profiles from the underlying atmospheric physics. Fits of these models to actual data ranged from poor to excellent, with many cases of what might be termed 'adequate but unsatisfying. Later modeling efforts added parameterized atmospheric mixing and cloud holes to try and improve the fits. While the improvements have been promising, comparisons of multiple models to a single dataset have been sparse, and tests against benchmark objects with known masses or effective temperatures even sparser. For these reasons no single model has emerged as the de facto standard; rather, each theory group continues to use their own cloud approach. Partly for this reason, model-derived effective temperatures and gravities for specific objects have an air of uncertainty as the results are not easily reproduced. I offer some suggestions for improving the current situation. While further model refinements are definitely needed, inversion methods which derive the atmospheric thermal profile, gravity, and cloud properties directly from all available data are certainly required. While such approaches have their own uncertainties, they will provide a cross check for forward models and will regularize the reporting of derived brown dwarf properties. The combination of inverse methods and forward models applies to benchmark systems with highly constrained properties is almost certainly the best path forward.

10. Constraining the Properties of the Dust Haze in the Atmospheres of Young Brown Dwarfs (Kay Hiranaka)

Brown dwarfs and exoplanets share physical properties: they both have radii similar to Jupiter and cool temperatures. Warm, young brown dwarfs ($\sim$2000K, $<$100 Myr) have thick clouds that affect emergent spectra and their clouds are likely to be similar to those of young gas giant planets. A better understanding of the role of clouds in brown dwarfs will inform our understanding of the thick clouds observed in directly imaged planets. It is thought that redder spectral energy distributions might indicate thick clouds, bluer spectral energy distributions might be thin or patchy clouds. We have combined observations and theory to make inroads on the process of disentangling the observed effects of the clouds. We use Mie theory to find the combination of dust properties that best reproduce the effects seen in the spectra of young brown dwarfs; in particular, we constrain the grain size distribution and the grain composition in young, warm brown dwarf clouds. The combination of Mg_2SiO_4 and the Hansen distribution with mean particle size of 0.1–0.3 μm fits the data best. This result suggests that young brown dwarfs may have silicate dust hazes with mean grain sizes much smaller than the regular cloud grains ($\sim$10 μm).

11. Building a Volume-Limited Sample of L/T Transition Dwarfs with Pan-STARRS and *WISE* (William Best)

Brown dwarf photospheres are dominated by molecules and dusty condensates that undergo significant chemical changes as they cool (e.g., Burrows et al. 2001). This is particularly true in the L/T transition (spectral types ≈L6–T4.5, temperatures $\approx 1400 - 1200$ K), where the condensate clouds that characterize L dwarfs fall below the photosphere via a process that is not yet understood (e.g., Burrows et al. 2006; Saumon & Marley 2008), making L/T transition dwarfs ideal for case studies of cloud formation and gas chemistry in ultracool atmospheres. However, state-of-the-art evolutionary and atmospheric models typically yield inaccurate luminosities and inconsistent temperatures for L/T objects with known masses and/or age determinations (e.g., Dupuy et al. 2009, 2010). A volume-limited sample of L/T transition dwarfs with accurate luminosities would considerably improve our ability to test the models.

Multiple searches over the past 15 years have found well over a thousand brown dwarfs, but with varying sensitivity, spatial coverage, and spectral completeness. Most searches have been incomplete for L/T transition dwarfs because these objects are optically faint and have near-infrared colors that are difficult to distinguish from M and early-L dwarfs (e.g., Burgasser et al. 2002a; Reid et al. 2008). Past searches sensitive to L/T objects have also focused on modest areas of the sky (e.g., Chiu et al. 2006; Day-Jones et al. 2013).

We have searched 30,000 deg^2 for L/T transition dwarfs using the optical Pan-STARRS1 3π (PS1) and mid-infrared *WISE* All-Sky surveys, cross-matching these catalogs to produce a unique multi-wavelength database. A detailed description of the PS1 and *WISE* surveys and initial results from our search can be found in Best et al. (2013). Briefly, we identified candidate L/T dwarfs through a series of quality, color, and magnitude cuts applied to our merged PS1+*WISE* database, followed by visual inspection of PS1, 2MASS, and *WISE* images. The unique $y_{\mathrm{P1}} - W1$ color proved to be especially helpful in distinguishing L/T transition dwarfs from background objects (Figure .7). We then obtained low-resolution near-infrared spectra for our candidates using IRTF/SpeX, and typed the spectra using the L and T dwarf standards from Kirkpatrick et al. (2010) and Burgasser et al. (2006). We identified a cut equivalent to a distance of 25 pc on the $W1$ vs. $W1 - W2$ color-magnitude diagram of L/T objects with known parallaxes, and used this along with our new discoveries to identify a volume-limited sample of L/T transition dwarfs.

We obtained spectra for 142 candidates. In total, we discovered 131 new ultracool dwarfs (spectral types M6 and later; Figure .7). 80 of these are L/T transition dwarfs, making ours the largest and most efficient search to date for these elusive objects (Best et al. 2013, and in prep). 28 of the L/T dwarfs have photometric distances less than 25 pc. With these and previously known objects we define a volume-limited set of L/T transition dwarfs with 25 pc. This set is mostly complete for declinations $-30° < \delta < 60°$ and galactic latitudes $|b| > 15°$.

Our discoveries help to form a well-defined, robust sample of L/T transition dwarfs that can constrain atmospheric models and improve our understanding of the progression from dusty and cloudy L dwarfs to clear T dwarf photospheres. For example, one of the more successful ultracool atmospheric models is the "hybrid" model of Saumon & Marley (2008), who use a smoothly-increasing cloud sedimentation parameter to model the depletion of clouds across the L/T transition. Their model predicts a "pileup" of objects in the middle of the L/T transition where the cooling slows as cloud depletion releases entropy trapped below the photosphere, a feature not seen in other models. Dupuy & Liu (2012) tentatively

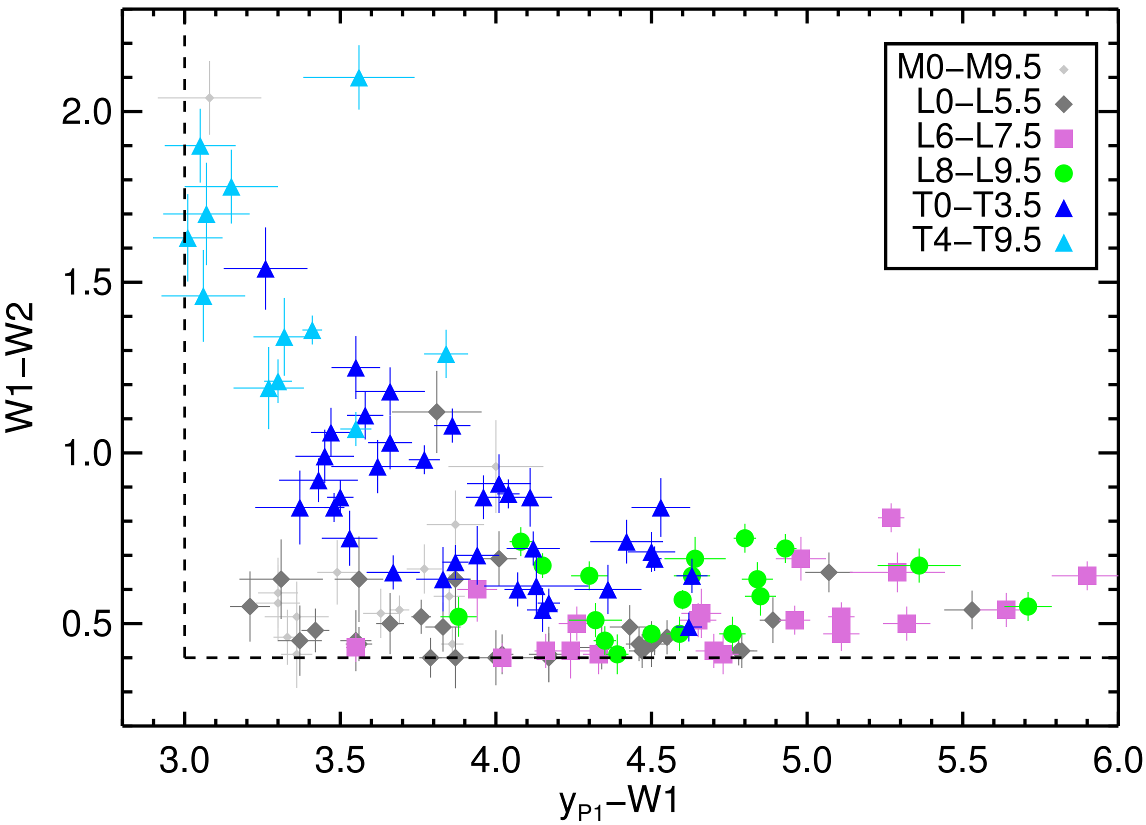

Figure .7: $W1 - W2$ vs. $y_{P1} - W1$ diagram for our new ultracool dwarf discoveries, which spanned spectral types M6–T7. The black dashed lines indicate color cuts we used to select our candidates. The $y_{P1} - W1$ color distinguishes the later L dwarfs (magenta squares and green circles) from most earlier-type L and M dwarfs, which near-infrared colors are not able to do.

detect this pileup, as well as a "gap" with few objects (i.e., a short-lived evolutionary phase) just after the pileup, but their sample is not volume-limited and contains only 36 objects. We will use our larger, volume-limited sample to constrain the nature of this gap and pileup, an important step towards understanding the structure of the L/T transition.

12. Variability in T and Y Dwarfs from Patchy Clouds and Hot Spots (Caroline Morley)

Brown dwarfs of nearly all spectral types—both inside and outside of the L/T transition—have been observed to be variable. Previous studies have focused on the high amplitude variable objects at the L/T transition, at temperatures where the iron and silicate clouds dissipate (Zhang & Showman 2014; Radigan et al. 2012). However, objects outside of this transitional effective temperature regime also exhibit variability (Buenzli et al. 2012; Buenzli et al. 2014; Radigan et al. 2014). This photometric variability may be due to patchy cloud cover, in which one hemisphere has a higher fraction of the surface covered in clouds. However, it could also be due, at least in part, to temperature perturbations in the atmosphere (Robinson & Marley 2014). These perturbations could be caused by 3D circulation patterns or by the radiative effect of cloud formation and breakup on the temperature structure of the atmosphere (Showman & Kaspi 2013).

We have presented models of the spectral dependence of variability in these two cases—patchy clouds and hot spots—for mid-late T dwarfs and Y dwarfs (Morley et al. 2014b). These include patchy salt, sulfide, and water ice clouds (Morley et al. 2012; Morley et al. 2014a). For objects over 375 K, patchy cloud opacity would generate the largest amplitude variability within near-infrared spectral windows. For objects under 375 K, water clouds generate larger amplitude variability in the mid-infrared.

Hot spots are modeled by adding energy to the model at different pressure levels, which creates a temperature perturbation to the pressure–temperature profile. These hot spots, in contrast to the patchy clouds, generate the largest amplitude variability at wavelengths within strong absorption features, between near-infrared spectral windows. The variability is highest amplitude at wavelengths that probe pressure levels at which the heating is the strongest.

Observations to understand the cause of variability in brown dwarfs must be able to distinguish between these two mechanisms. Therefore, the most illustrative types of observations for understanding the physical processes underlying brown dwarf variability are simultaneous, multi-wavelength observations that probe both inside and outside of molecular absorption features.

13. Clouds and hazes in hot Jupiter Atmospheres: Results from a large HST program (David Sing)

Clouds and hazes have become an emerging and ever-growing important topic for highly-irradiated hot-Jupiter exoplanets. These aerosol species can be effectively probed with transmission spectroscopy in addition to albedo measurements for transiting planets. I present the various lines of evidence for upper atmospheric haze in the canonical hot Jupiter HD 189733b, and note several possible links to brown dwarf atmospheres. In addition, there is evidence for similar clouds and hazes in other hot Jupiters, new results which are now emerging from a large Hubble Space Telescope program covering eight exoplanets.

Acknowledgements. The splinter organizers would like to thank the CS18 Science Organizing Committee for providing a forum to discuss these issues. W. Best is grateful to the Pan-STARRS1 builders, observing and processing staff for creating the rich new PS1 catalog. E. Buenzli acknowledges support by the Swiss National Science Foundation (SNSF). A. Rajan acknowledges the MMT, NTT and UKIRT telescope staff for all their assistance in collecting the data. A. Showmman acknowledges support from NSF grant AST1313444. X. Zhang acknowledges support by Bisgrove Scholar Program.

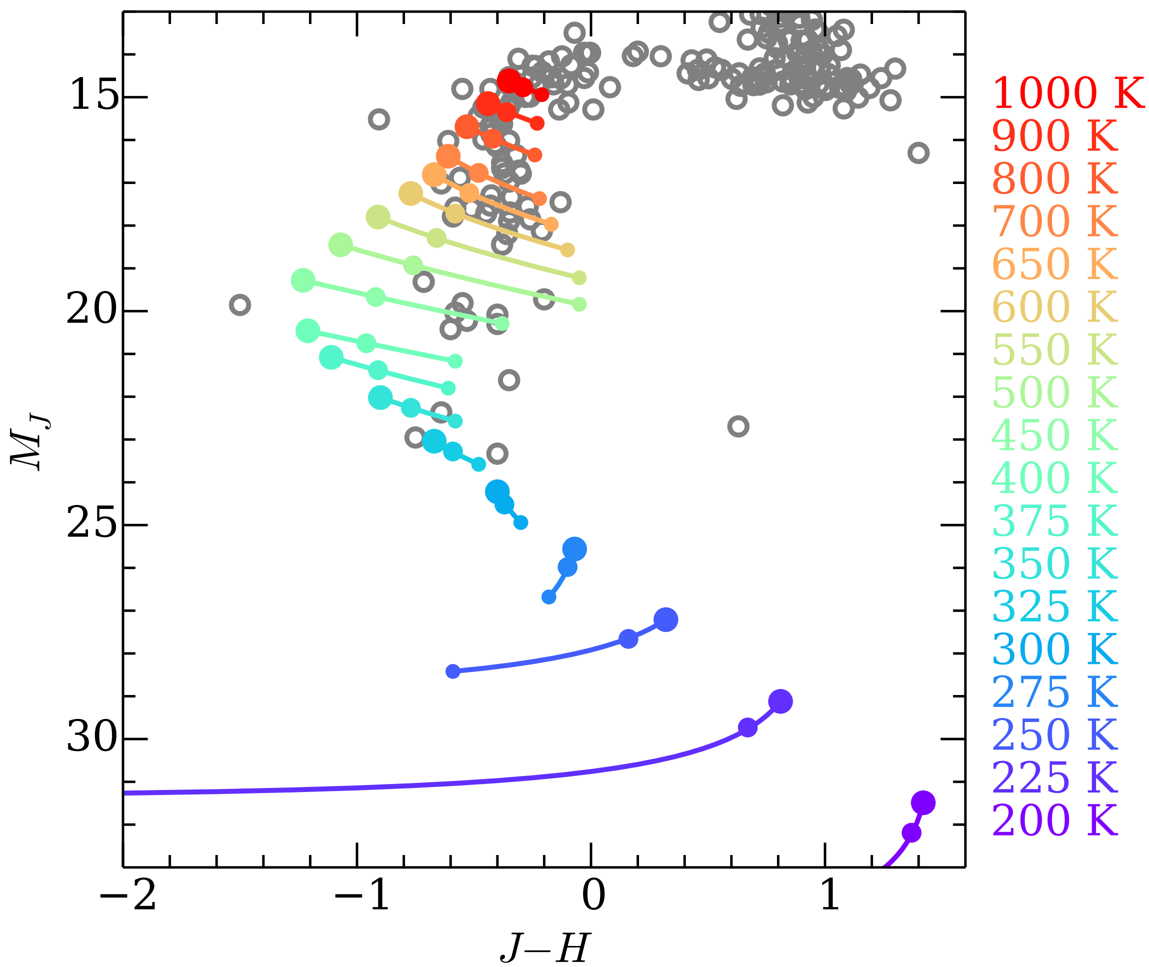

Figure .8: Color–magnitude diagram ($J - H$ vs. M_J) for partly cloudy models. The center medium-sized dot represents the 50% cloudy model in radiative–convective equilibrium. The connected large and small dots show the photometry of the clear and cloudy columns respectively. The $T_{\rm eff}$ corresponding to each color is shown on the right of each panel. The observed brown dwarfs with distance measurements are shows as gray open circles (Dupuy & Liu 2012).

References

Ackerman, A. S., & Marley, M. S. 2001, ApJ, 556, 872

Apai, D., Radigan, J., Buenzli, E., et al. 2013, ApJ, 768, 121

Artigau, É., Bouchard, S., Doyon, R., & Lafrenière, D. 2009, ApJ, 701, 1534

Bailer-Jones, C. A. L., & Mundt, R. 1999, A&A, 348, 800

Best, W. M. J., Liu, M. C., Magnier, E. A., et al. 2013, ApJ, 777, 84

Biller, B. A., Crossfield, I. J. M., Mancini, L., et al. 2013, ApJ, 778, L10

Buenzli, E., Apai, D., Morley, C. V., et al. 2012, ApJ, 760, L31

Buenzli, E., Apai, D., Radigan, J., Reid, I. N., & Flateau, D. 2014, ApJ, 782, 77

Burgasser, A. J., Kirkpatrick, J. D., Brown, M. E., et al. 2002a, ApJ, 564, 421

Burgasser, A. J., Marley, M. S., Ackerman, A. S., Saumon, D., Lodders, K., Dahn, C. C., Harris, H. C., & Kirkpatrick, J. D. 2002b, ApJ, 571, L151

Burgasser, A. J., Geballe, T. R., Leggett, S. K., Kirkpatrick, J. D., & Golimowski, D. A. 2006, ApJ, 637, 1067

Burgasser, A. J., Gillon, M., Faherty, J. K., et al. 2014, ApJ, 785, 48

Burrows, A., Hubbard, W. B., Lunine, J. I., & Liebert, J. 2001, Rev Mod Phys, 73, 719

Burrows, A., Sudarsky, D., & Hubeny, I. 2006, ApJ, 640, 1063

Chiu, K., Fan, X., Leggett, S. K., et al. 2006, AJ, 131, 2722

Clarke, F. J., Hodgkin, S. T., Oppenheimer, B. R., Robertson, J., & Haubois, X. 2008, MNRAS, 386, 2009

Crossfield, I. J. M., Biller, B., Schlieder, J. E., et al. 2014, *Nature* , 505, 654

Day-Jones, A. C., Marocco, F., Pinfield, D. J., et al. 2013, MNRAS, 430, 1171

Dupuy, T. J., & Liu, M. C. 2012, ApJS, 201, 19

Dupuy, T. J., Liu, M. C., Bowler, B. P., et al. 2010, ApJ, 721, 1725

Dupuy, T. J., Liu, M. C., & Ireland, M. J. 2009, ApJ, 699, 168

Enoch, M. L., Brown, M. E., & Burgasser, A. J. 2003, AJ, 126, 1006

Faherty, J. K., et al. 2012, ArXiv e-prints

Freytag, B., Allard, F., Ludwig, H., Homeier, D., & Steffen, M. 2010, A&A, 513, A19+

Gelino, C. R., Marley, M. S., Holtzman, J. A., Ackerman, A. S., & Lodders, K. 2002, ApJ, 577, 433

Gillon, M., Triaud, A. H. M. J., Jehin, E., Delrez, L., Opitom, C., Magain, P., Lendl, M., & Queloz, D. 2013, A&A, 555, L5

Girardin, F., Artigau, É., & Doyon, R. 2013, ApJ, 767, 61

Goldman, B., et al. 2008, A&A, 487, 277

Kirkpatrick, J. D., Looper, D. L., Burgasser, A. J., et al. 2010, ApJS, 190, 100

Koen, C. 2003, MNRAS, 346, 473

Koen, C., Matsunaga, N., & Menzies, J. 2004, MNRAS, 354, 466

Marley, M. S., Saumon, D., & Goldblatt, C. 2010, ApJ, 723, L117

Metchev, S., Apai, D., Radigan, J., et al. 2013, Astronomische Nachrichten, 334, 40

Morley, C. V., Fortney, J. J., Marley, M. S., et al. 2012, ApJ, 756, 172

Morley, C. V., Marley, M. S., Fortney, J. J., et al. 2014, ApJ, 787, 78

Morley, C. V., Marley, M. S., Fortney, J. J., & Lupu, R. 2014, ApJ, 789, L14

Radigan, J., Jayawardhana, R., Lafrenière, D., et al. 2012, ApJ, 750, 105

Radigan, J., Lafrenière, D., Jayawardhana, R., & Artigau, E. 2014, ArXiv e-prints, arXiv:1404.3247

Rajan, A., Patience, J., Wilson, P. A. et al. 2014, MNRAS, submitted

Reid, I. N., Cruz, K. L., Kirkpatrick, J. D., et al. 2008, AJ, 136, 1290

Robinson, T. D., & Marley, M. S. 2014, ApJ, 785, 158

Saumon, D., & Marley, M. S. 2008, ApJ, 689, 1327

Saumon, D., Marley, M. S., Abel, M., Frommhold, L., & Freedman, R. S. 2012, ApJ, 750, 74

Showman, A. P., & Kaspi, Y. 2013, ApJ, 776, 85

Tinney, C. G., & Tolley, A. J. 1999, MNRAS, 304, 119

Wilson, P. A., Rajan, A., & Patience, J. 2014, A&A, 566, A111

Zhang, X., & Showman, A. P. 2014, ApJ, 788, L6

(Left to right) John Bochanski, Andrew West, Jackie Faherty, Adam Burgasser, Daniella Bardalez Galgiuffi, Sarah Logsdon.